[3] Press, H. and Houbolt, J. C., "Some Applications of Generalized Harmonic Analysis to Gust Loads on Airplanes," I.A.S. Preprint No. 449, 1954.
[4] Lin, Y. K., "Transfer Matrix Representation of Flexible Airplanes in Gust Response Study," *Journal of Aircraft*, Vol. 2, No. 2, March–April 1965, pp.116–121.
[5] Fuller, J. R., "A Procedure for Evaluating the Spanwise Variations of Continuous Turbulence on Airplane Responses," *Journal of Aircraft*, Vol. 5, No. 1, Jan.–Feb. 1968, pp. 49–52.
[6] Diederich, F. W., "The Dynamic Response of a Large Airplane to Continuous Random Atmospheric Disturbances," *Journal of the Aeronautical Science*, Vol. 23, Oct. 1956, pp. 917–930.
[7] Eichenbaum, F. D., "A General Theory of Aircraft Response to Three-Dimensional Turbulence," *Journal of Aircraft*, Vol. 8, No. 5, May 1971, pp. 353–360.
[8] Coupry, G., "Etude Critique des Méthodes de Calcul de la Fonction de Transfert d'un Avion à la Turbulence Atmosphérique," Comptes Rendus de l'Académie des Sciences, Paris, Tome 271, Ser. A, 1970, pp. 46–49.
[9] Taylor, J., "Manual on Aircraft Loads," AGARDograph 83, Pergamon Press, New York, 1956, pp. 200–202.
[10] Rice, S. O., "Mathematical Analysis of Random Noise," *Bell System Technical Journal*, Vol. 23, No. 3, 1944, Pts. I and II, pp. 282–332; also Vol. 24, No. 1, 1945, Pts. III and IV, pp. 46–156.

AUGUST 1972 J. AIRCRAFT VOL. 9, NO. 8

A General Class of Exact Airfoil Solutions

RICHARD M. JAMES*
Douglas Aircraft Company, Long Beach, Calif.

Existing classical analytical airfoil solutions are not flexible enough to provide sufficiently critical test problems for modern numerical techniques. This paper presents the theory and some results for a very general and versatile form of conformal mapping which can be used to generate local analytical bumps and dips on airfoil profiles. The mapping uses an analytical modulating function constructed from multipoles within the unit circle, and various consequences of this format are presented—where they may have an influence on numerical test cases. For instance, the existence of curvature singularities at the trailing edges of most common airfoils (Joukowski, Von Mises, Karman-Trefftz, etc.) is made particularly evident. Results are presented for zero trailing edge angle from an IBM 2250 Graphics Display System, showing how a variety of severe test problems with exact solutions and involving local surface deformations can be generated at will.

Introduction

THE continual growth of well-founded modern numerical techniques has focused attention on details and accuracy considerations that were not important in the earlier days of their gross development. Furthermore, the widespread and general reduction of funding available to support ill-founded and wasteful schemes has generated timely interest in efficiency and maximum accuracy for a given computing time.

Many examples of this changing emphasis have occurred within the daily working life of engineers at Douglas, and provide a very clear case for the development of "exact" solutions adequate to investigate the detailed performance of numerical methods. For instance: a) the Douglas–Neumann[1] program is one of the major fully established tools for low-speed flow problems in the aircraft and associated industries. Even though the method is formally exact in two and three dimensions, the discretization used in practice leads very frequently to questions about the point spacing density required to extract sufficient flow detail in regions of rapid geometrical change. Typical practical cases are local lumps, thin trailing edges, close approach of slat trailing edges to main airfoils, very sharp noses, etc. b) Recent new methods[2, 3] for airfoil problems where attention has been directed toward accuracy rather than generality of body shape (because of the subsequent intention to develop compressible versions) have intensified the need for adequate test problems. In the flow analysis part of Ref. 2, and in Ref. 3, the surface angle has to be extracted from coordinate data and its accuracy is an absolute limitation on convergence of the iterative cycle in both. For very sharp noses, or excessive camber, or flap hinge lumps—some guidance is needed on input detail and on the flow response to it. c) The design of high-lift airfoils by the methods of Ref. 2 according to the precepts of Ref. 4 have led to frequent discrepancies and futile speculations on accuracy between the various methods mentioned previously. These high-lift airfoils are very cambered, have sharp noses and unsmooth pressure distributions. Of course, the need is again to have some kind of "exact" solution which incorporates these features. d) Finally, there remains the possibly most important application of all, namely, guidance for the questions which arise from pure data-handling of geometry. For given coordinate data the production of "smoothed" input points, to say nothing of angles and curvature, remains a very real and difficult problem in spite of the abundance of numerical techniques. A number of point-spacing suggestions have been proposed for use with the Douglas-Neumann program and these usually involve arc length and curvature; which require in turn interpolation and differentiation of possibly noisy coordinate data. Hence, there is a natural concern with smoothing and associated numerical operations; but, again, it is effectively impossible to assess the various alternatives without being able to generate test cases. How many points are required to define a slat nose? How many if the data is noisy? and what should be their spacing? Such questions can only be approached (never mind answered) by starting with a sufficiently unpleasant geometry and adding

Received December 16, 1971; revision received March 23, 1972. This work was supported by the McDonnell Douglas Independent Research and Development Program.
Index category: Airplane and Component Aerodynamics.
* Senior Engineer/Scientist, Aerodynamics Research Group, Douglas Aircraft Company, Long Beach.

noise. Clearly a, b, c, and d are more than sufficient to establish the need for flexible exact solutions, preferably obtained in the classical conformal mapping style because then the geometry and flow aspects can be decoupled. However, on turning to the usual tests, the engineer is confronted with the fact that not only are Joukowski, Karman-Trefftz, Von Mises (etc.) airfoils incapable of satisfying the needs of a, b, c, and d; but also the accounts given are frequently semi-geometrical confusing and lack unity.

Consequently, this paper is devoted to the attempt to describe briefly the class of airfoils known as "pole" airfoils which do have the required flexibility. The account given below is orientated toward simplicity and unity. More detail can be obtained from Ref. 5.

Basic Mapping Format

As pointed out in the introduction, the classical mapping procedures, although well-known, lack unity in presentation. For the simplest type of mapping in which the complex potential is transferred in a one-to-one relationship between a $z = x + iy$ plane containing the real airfoil and a $\zeta = \xi + i\eta$ plane containing a circle, this unity comes immediately from the constraints. By being careful with the constraints it is possible to make the mapping format very simple, thus making generalization correspondingly easy. A certain amount of elementary background cannot be avoided if only to establish a notation, so the opportunity has been taken in this section to give a very brief description of the ideas in the "unifying" style.

Since the flow potential ϕ and stream function ψ satisfy the Cauchy–Riemann equations, the complex velocity q and complex potential w are related by

$$q = u - iv; \qquad w = \phi + i\psi; \qquad q = dw/dz \tag{1}$$

and then, in the usual way

$$q = \frac{dw}{d\zeta} \Big/ \frac{dz}{d\zeta} \tag{2}$$

where $(dz/d\zeta)$ is the mapping derivative and $(dw/d\zeta)$ is the complex velocity ($\tilde{q}$, say) in the circle plane.

Equation (2) already makes it clear that attention should be directed toward the mapping derivative specified explicity as a function of ζ, because $\tilde{q}(\zeta)$ is essentially known, and the whole point of mapping is to solve the problem on an easy shape (i.e., the circle). Furthermore, the velocities in the two planes are required to reduce to the same freestream at great distances from the disturbances and then it follows from (2) that

$$dz/d\zeta \to 1 \quad \text{as} \quad |z|, |\zeta| \to \infty \tag{3}$$

The requirements that the actual flow in the z-plane does not contain stagnation points, nor infinite velocities, nor multiple values off the airfoil surface make it clear that the mapping derivative is severely constrained in form for the domain $|\zeta| > 1$ (i.e., outside the circle). In fact, since these "flow reality" conditions are certainly satisfied by $\tilde{q}(\zeta)$, then

$$dz/d\zeta \text{ is regular and nonzero for } |\zeta| > 1 \tag{4}$$

Although this has been deduced from flow reality considerations, it is also intimately connected with the nonappearance of geometrical peculiarities as will be seen.

Turning next to conditions on the airfoil surface, it is well-known that a finite wedge angle of included angle τ can be "opened out" by a local factor of the form

$$z - z_0 \sim (\zeta - \zeta_0)^{2-\tau/\pi}$$

from which it is clear that, if $dz/d\zeta$ is to map a wedge trailing edge into a locally circular region, then it must contain a factor of the form

$$dz/d\zeta = (1 - \zeta_0/\zeta)^{1-\tau/\pi} \cdot \quad \text{(smooth function)} \tag{5}$$

which is a convenient way to express it, since the factor also $\to 1$ as $|\zeta| \to \infty$.

In the case of aerodynamics, however, there is an additional feature in that, according to the Kutta-Joukowski hypothesis, the flow velocity must remain finite at the trailing edge. Therefore, since $\tilde{q}(\zeta)$ has a zero at the rear stagnation point on the circle it follows from Eqs. (2) and (5) that this rear stagnation point must coincide with ζ_0. The front stagnation point is not affected and so, if no other sharp edge is required to be mapped, the mapping derivative should not contain any other singular factor than shown in Eq. (5). Thus, without loss of generality, the rear stagnation point can be taken as $\zeta = 1$ and then

$$dz/d\zeta = (1 - 1/\zeta)^{1-\tau/\pi} g(\zeta) \tag{6}$$

As a consequence, the modulating function $g(\zeta)$ must clearly satisfy the following:

$$g(\zeta) \to 1 \quad \text{as} \quad |\zeta| \to \infty \tag{7a}$$

$$g(\zeta) \text{ is regular and nonzero for } |\zeta| > 1 \tag{7b}$$

$$g(\zeta) \text{ has no zeros or poles on } |\zeta| = 1 \tag{7c}$$

In addition, the closure condition for conventional airfoils can be expressed in terms of the ζ-plane by

$$\int_C \frac{dz}{d\zeta}\, d\zeta = 0 \tag{8}$$

where C is any contour enclosing the unit circle.

Regular and Pole Airfoils

The conditions laid down in Eqs. (7) and (8) are easy to satisfy in very general terms. For instance, a suitable form of $g(\zeta)$ consists of poles scattered within the unit circle, e.g.,

$$g(\zeta) = 1 + \frac{\lambda_{11}}{\zeta - d_{11}} + \frac{\lambda_{12}}{\zeta - d_{12}} + \cdots \frac{\lambda_{21}}{(\zeta - d_{21})^2} + \cdots \frac{\lambda_{31}}{(\zeta - d_{31})^3} + \cdots \tag{9}$$

which can also be expressed as a rational fraction

$$g(\zeta) = \frac{(\zeta - c_{11})^{\alpha_1}(\zeta - c_{12})^{\alpha_2} \cdots}{(\zeta - d_{11})(\zeta - d_{12}) \cdots (\zeta - d_{21})^2 \cdots} \tag{10}$$

For most purposes, Eq. (9) is the more convenient and (e.g.) makes it clear that the first of constraints Eq. (7) is satisfied. The other two are satisfied also if

$$|d_{ij}| < 1, \qquad |c_{ij}| < 1 \tag{11}$$

Airfoils defined by this kind of modulating function have been called "pole" airfoils and include many common types as special cases. For instance, Joukowski, Von Mises and Carafoli[6] profiles are examples of pole airfoils with $\tau = 0$ or π.

It is worth drawing attention to the fact that this system also defines the associated airfoils with $\tau \neq 0$; that is, those airfoils whose general character (camber, thickness, waviness, etc.) are controlled by the same set of parameters as for $\tau = 0$. No such uniformity is available for the other classical wedge trailing edge airfoils, whose parametric dependences can become very involved. Consequently, it is convenient to generalize the class even further for discussion purposes to include any airfoil whose $g(\zeta)$ has a Taylor expansion at every point of $|\zeta| = 1$. Such airfoils will be called "regular" and and clearly every pole airfoil is a "regular" airfoil.

However, not every regular airfoil is a pole airfoil, because (for instance) the bookkeeping involved in extracting the factor $(1 - 1/\zeta)^{1-\tau/\pi}$ could just as well have extracted a factor of the form $[(1 - \zeta)/(\zeta + a)]^{1-\tau/\pi}$, so that the result would not

be a pole airfoil according to Eqs. (6) and (9). Typical of this class are Karman-Trefftz and Piercy[7,8] airfoils.† The extended class is not useful computationally because the extended requirement on $g(\zeta)$ is too general to be conveniently programed. Nevertheless, certain very important properties hold for all regular airfoils, not merely pole airfoils and one that is important for numerical test cases is the existence of a curvature singularity at the trailing edge. This is discussed in the next section.

Most of the remainder of this work is connected with the properties of pole airfoils of which the best-known member would be the Joukowski airfoil. In the pole format a Joukowski profile looks unfamiliar, but simpler. By paying attention to the circle which is to be mapped and insisting that the origin of coordinates in the z-plane shall be the trailing edge, it is not difficult to show[5] that the center of the so-called "mapping circle" is the pole location in the ζ-plane, and that the Joukowski mapping is then

$$z = (\zeta - 1)^2/(\zeta - d) \tag{12}$$

from which

$$dz/d\zeta = (1 - 1/\zeta)[1 + 1/(\zeta - d) + d(1 - d)/(\zeta - d)^2] \tag{13}$$

Hence, a Joukowski airfoil has a single and double pole at the same point and so cannot be considered the simplest pole airfoil.

This distinction is reserved for the single-pole airfoil characterized, not surprisingly, by

$$dz/d\zeta = (1 - 1/\zeta)[1 + 1/(\zeta - d)] \qquad (\text{when } \tau = 0) \tag{14}$$

Although this is formally simpler than Eq. (13) the actual $z(\zeta)$ relation is more involved than Eq. (12); but the control of thickness, camber and so on is still dependent on only the one parameter d. In Ref. 5, some comparisons between these two simple airfoil types are given, and it is not possible to pursue this topic here even though the single-pole airfoil is used later as a basis for testing certain geometrical artifices.

For Eqs. (13) and (14), it can be seen that the strength of the first-order pole is unity. This is a consequence of the closure condition (8) which leads to

$$\sum_{k=1}^{N} \lambda_{1k} = 1 - \tau/\pi \tag{15}$$

when applied to Eqs. (6) and (9). Hence, not only must the strengths of the first-order poles sum to unity (when $\tau = 0$), but it is also implied that at least one pole must be present in which case its strength must be unity [viz. Eq. (14)].

Turning from the simplest possible cases to previous attempts at generalization, the most versatile are the Von Mises profiles ably described in Ref. 9. In the format of this paper they can be expressed by

$$\frac{dz}{d\zeta} = \left(1 - \frac{k_0}{\zeta - d}\right)\left(1 - \frac{k_1}{\zeta - d}\right)\left(1 - \frac{k_2}{\zeta - d}\right)\cdots = \left(1 - \frac{1}{\zeta}\right)\left[1 + \frac{1}{\zeta - d} + \frac{a_2}{(\zeta - d)^2}\cdots\right] \tag{16}$$

which is an appreciable generalization of the Joukowski profiles. Rauscher[9] shows a few examples of manipulation of the zeros to give different shapes, but it is clear that the generality of Eq. (16) is constrained by the fact that all the poles are in the same location.

There is no obvious a priori reason to suppose that this restriction in Eq. (16) is important; however, the major purpose of this paper is to show that the more versatile pole airfoil format (9) enables the creation of local surface deformations just because the ability to select both poles and zeros is preserved.

† The author is indebted to W. R. Sears for drawing his attention to some of these less well-known profiles as in Refs. 6, 7 and 8. However, no exhaustive bibliographic study can be claimed for this paper.

Trailing Edge Singularities

As pointed out before one important aspect of these exact solutions obtained by conformal mapping is the singularities created by the use of complex variables and analytic functions. In testing flow solutions from (say) the Douglas-Neumann program and comparing with other numerical methods based more closely on a knowledge of mapping, it is clearly important to know exactly how the flow behaves in detail. Furthermore, in constructing alternative methods, local flow singularities often have to be extracted analytically so that a knowledge of the local "inner expansion" is important.

With regard to regular airfoils—which include every common test case—there exists a curvature and velocity singularity at the trailing edge such that although a local wedge may occur with the associated flow, the extent of this effect is not as expected. The mechanism for this follows quite naturally from the assumption that $g(\zeta)$ is regular and nonzero at $\zeta = 1$ in Eq. (6). Thus, using a subscript s to denote "surface values" and

$$\zeta_s = e^{i\omega} \qquad (0 \le \omega \le 2\pi)$$

it is clear that on the surface locally

$$g(\zeta_s) = g(1) + (\zeta_s - 1)g'(1) + \cdots \tag{17}$$

where $g(1)$ cannot be zero by hypothesis.

Also, using σ to denote arc length measured along the profile from the trailing edge and χ to denote the surface inclination, the connection between these surface parameters and the mapping derivative is provided by

$$\frac{d\sigma}{d\omega} = \left|\left(\frac{dz}{d\zeta}\right)_s\right|; \qquad \chi = \frac{\pi}{2} + \omega + \operatorname{Arg}\left(\frac{dz}{d\zeta}\right)_s \tag{18}$$

Using Eqs. (18) and (17) in Eq. (6), the local behavior of arc length in terms of a small angular displacement:

$$\begin{aligned} \varepsilon &= \omega \quad (\text{upper surface}) \\ &= 2\pi - \omega \quad (\text{lower surface}) \end{aligned}$$

can easily be expressed as

$$\frac{d\sigma}{d\omega} = \varepsilon^{1-\tau/\pi}\left\{|g(1)| \pm \frac{C}{|g(1)|}\varepsilon\cdots\right\} \qquad (+ \equiv \text{upper}) \tag{19}$$

where the constant C is a combination of real and imaginary parts of $g(1), g'(1)\cdots$ which can neither vanish nor be infinite. Or, in other words, Eq. (19) is an inevitable local decay law.

Integrating Eq. (19), leads to

$$\Delta\sigma = \varepsilon^{2-\tau/\pi}\{a_0 \pm a_1\varepsilon\cdots\} \tag{20}$$

where $\Delta\sigma$ represents the surface distance measured from the trailing edge, the $+$ sign denoting upper surface ($\omega = \varepsilon =$ small).

Similarly the surface angle can be expressed as

$$\begin{aligned} X &= b_0{}^{+} + \varepsilon b_1\cdots \quad (\text{upper}) \\ &= b^{-} - \varepsilon b_1\cdots \quad (\text{lower}) \end{aligned} \tag{21}$$

where b_1 is again nonzero and finite. Using the variable δ to denote the clumsy combination

$$\delta = (\Delta\sigma)^{1/(2-\tau/\pi)}$$

it follows from Eq. (20) that the series expressing δ as a function of ε can be reversed since the leading term cannot be zero, and then ε takes the form

$$\varepsilon = A_1\delta \mp A_2\delta^2\cdots \tag{22}$$

Thus the change of angle from the trailing edge value is given by Eq. (21) using Eq. (22) as

$$\Delta\chi = \pm C_1\delta \cdots = \pm C_1\Delta\sigma^{1/(2-\tau/\pi)} \cdots \qquad (23)$$

so that the curvature is locally described by

$$K_s \sim (\Delta\sigma)^{-(1-\tau/\pi)/(2-\tau/\pi)}$$
$$\sim (\Delta\sigma)^{-1/2} \quad \text{if} \quad \tau = 0$$

and this kind of singularity will always occur unless $\tau = \pi$, the completely blunted end.

Following a similar argument, the velocity can be shown to have an expansion in terms of ε of the type

$$|q_s| \sim \varepsilon^{\tau/\pi} \quad \{a_0 \mp a_1\varepsilon \cdots\}$$

so that using Eq. (22)

$$|q_s| \sim \delta^{\tau/\pi} \quad \{C_0 \pm C_1\delta \cdots\} \qquad (24)$$

and the first term is the usual wedge flow behavior showing an arc length dependence of the "power-law" type with exponent $(\tau/\pi)/(2-\tau/\pi)$. However, the remainder of the expression in { } depends on the unusual variable δ and not simple powers of $\Delta\sigma$. This, again, is a useful piece of information when available for such a general class of profiles, because the velocity end behavior frequently has to be extracted in otherwise smooth numerical techniques (see e.g., Ref. 2).

These results are not easy to visualize except that for the many plots of velocities on Joukowski airfoils available in the traditional literature, the local square-root "hook" at the trailing edge can be seen readily enough. Figures 1 and 2 show how the variations predicted by Eqs. (23) and (24) appear from some earlier computed examples and confirm these formulae. That is, according to Eq. (23) $\Delta\chi$ should be a linear function of $\Delta\sigma$ when $\tau = 0$, and according to Eq. (24), $|q_s|/\delta^{\tau/\pi}$ should be a linear function of δ. These results

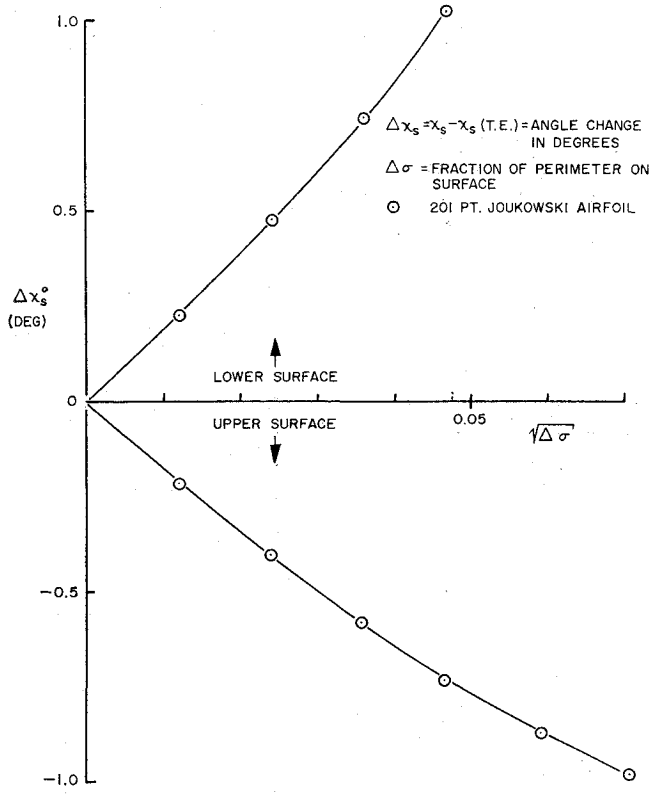

Fig. 1 Angle variation from trailing edge for a Joukowski airfoil as a function of square root of distance.

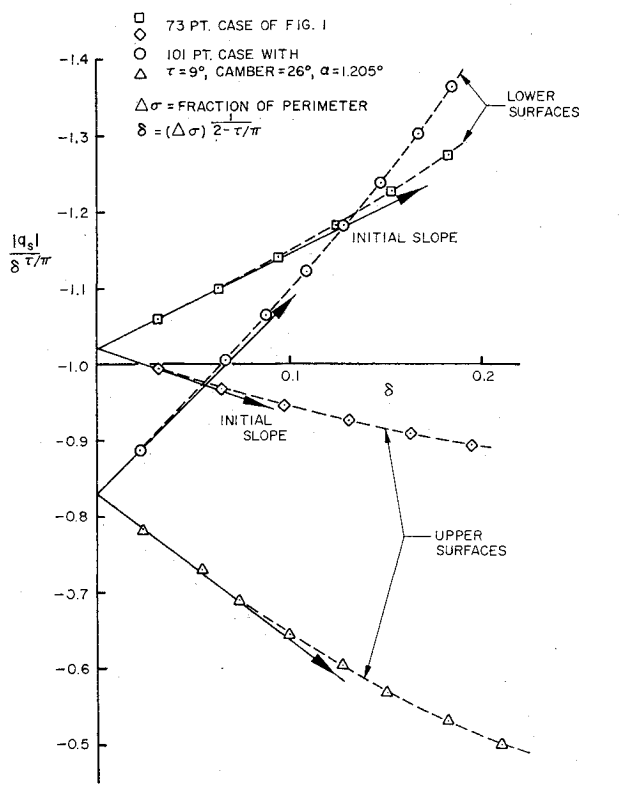

Fig. 2 Normalized velocity parameter near the trailing edge for two Karman-Trefftz airfoils as a function of a normalized distance parameter.

cannot be new per se, but they are certainly not well-known currently—particularly not in the general sense previously discussed.

General Computation

A computer program was written for the Douglas IBM 360/65 system for the case of zero trailing edge angle—since this is the easiest case and the ultimate value of the program was initially speculative. This program was subsequently modified for use with the IBM 2250 graphics display system in such a way that the operator could input pole orders, strengths and positions at the keyboard and then observe the shapes so defined.

From this information the computation involved consists of mere quadrature of Eqs. (6) and (9) involving only elementary steps. Various special cases, however, had to be isolated and the formal integral functions treated by local expansions. These correspond to combinations of $n = 1$ or >1, n large, and $|d|$ small—where n represents the order of the pole in question. The steps taken to ensure accurate computation under these circumstances are described in Ref. 5 and will not be considered further here. A similar remark applies to the calculation of arc length, angle, curvature and velocity—all of which are straightforward operations, though tedious. These quantities are available as standard printout, but the graphics display can be used to show the velocity distribution as a function of surface arc length for any chord angle of attack merely by pressing the appropriate keys.

However, one aspect of this system should be emphasized. Thus, one display available does show the locations of the poles selected in the circle plane and simultaneously provides a tabular picture. Errors can be minimized by this step, but the locations of the zeros are not shown and their positions are very important. For instance: a) a necessary condition (but not sufficient) for nonlooping of the airfoil contour is

that no zero shall lie outside the unit circle and b) conversely, looped or cusped shapes can be obtained quite readily by choosing a zero outside or on the unit circle. Statement a) is proved in Ref. 5 and b) is useful for testing general parametric curve fitting procedures, but the aerodynamics naturally becomes meaningless for looped contours. In particular, the restriction on the zeros of the mapping derivative is also necessary for the proper application of Blasius' theorem which is also discussed in Ref. 5 and not considered further here.

In any event, it is usually the case that zeros and poles are selected for a particular purpose. The pole strengths then have to be calculated externally and adjustments made to ensure satisfaction of the closure conditions [i.e., of (15)]. This step is easy to organize algebraically—it need not involve trial and error—but it is nevertheless, very tedious on a desk machine. This fact coupled with the relative expense of graphics operation, means that the current version of the program is not exactly usable as a daily routine item. Conversely, the results obtained (below) are all the more impressive for not being special favorable examples selected from a lot of trials.

Special Geometries

It is a routine matter to generate smooth normal airfoils and space will not be wasted to demonstrate this fact since, as already pointed out, the real virtue in this consolidation of airfoil mapping theory lies in the increased flexibility of the pole format which in turn provides a means for generating local effects to order. Furthermore, it must be obvious from the remarks of the preceding section that the desired technique for producing these effects must be rational to the point that it is easy to see how to discriminate *beforehand* between "lumps" and "dips" (e.g.) and also it must be simple enough to keep graphics system operating expenses within reason. The fact that the reduction to the form of Eq. (9) had to be done by hand, made sure that these criteria were met in this study.

The fact that a zero ($\zeta = c$) of $dz/d\zeta$ produces a local loop if $|c| > 1$ or a cusp if $|c| = 1$ has already been mentioned, and in Ref. 5 it is shown that if $|c|$ is just less than unity a lump with a parabolic tip is raised. These effects, however, are local in an essentially undefinable manner since the arguments on which they are based are themselves absolutely local (see Ref. 5). This conservatism had already been reflected in the preceding section in that the condition $|c| < 1$ was quoted as being necessary only. In practice, configurations with global loops which have every $|c_{ij}| < 1$ have been obtained, so that the conservative view is not merely academic. Attempts to find a way of generating local convolutions of preassigned type and location by bringing zeros close to the circle and balancing these perturbations by more or less arbitrary shifts of other zeros and poles (while maintaining closure) only served to reinforce this conservatism. It seems that intuition and common sense are very poor guides in this area, and operating in this way it proved to be extraordinarily difficult to foresee the final contour. Some horrible results are shown in Ref. 5.

Conversely the final procedure described here seems very simple as hindsight. Starting from a contour defined by

$$dz/d\zeta = (1 - 1/\zeta)\, g(\zeta) \tag{25}$$

let another factor $f(\zeta)$ be applied so that the new shape given by

$$dz'/d\zeta = (1 - 1/\zeta)\, g(\zeta) f(\zeta) \tag{26}$$

has the desired local properties. For the sake of over-all simplicity and particularly to make the new closure conditions easy, let $f(\zeta)$ be such that z' is also a pole airfoil. Then $f(\zeta)$ must itself be decomposable into poles. Since a zero of $f(\zeta)$ must be close to the surface, a factor $(\zeta - c)$ will be needed and this will mean inclusion of another pole factor $(\zeta - d)$. Hence, the simplest reasonable form of $f(\zeta)$ would be

$$f(\zeta) = (\zeta - c)/(\zeta - d) \tag{27}$$

Now, if c and d have the same argument, then it is easy to show that their combined influence will tend to produce an initially inward indented contour if $|c| < |d|$ and outward if $|c| > |d|$. Of course, if $|c| = |d|$, there will be no effect so adequate localization ought to result if $|c| \sim 1$ and $|d| \sim |c|$.

However, a single factor of form (27) will not do, for if it is expressed as

$$1 + \mu/(\zeta - d) \qquad (\mu = d - c)$$

the effect on the first-order poles of $g(\zeta)$ can be written as $\tilde{g}(\zeta)$ where

$$\tilde{g}(\zeta) = \left(1 + \frac{\lambda_1}{\zeta - d_1} + \frac{\lambda_2}{\zeta - d_2} \cdots \frac{\lambda_N}{\zeta - d_N}\right)\left(1 + \frac{\mu}{\zeta - d}\right)$$

giving rise to the modified closure condition

$$\mu + \sum_{k=1}^{N} \lambda_k = 1 \tag{28}$$

But the original closure condition required that the sum of the first-order pole strengths was, itself, unity. Hence, Eq. (28) means that $\mu = 0$.

A double factor of form (27), namely

$$f(\zeta) = [(\zeta - c)/(\zeta - d)] \cdot [(\zeta - d')/(\zeta - d')] \tag{29}$$

turns out to be satisfactory. If again (c',d') lie on the same radial line close together but relatively distant from (c,d), the action of (c,d) should not be excessively distorted from that previously discussed. Simultaneously, sufficient extra parameters are provided to ensure closure. In order to see that this is so, write Eq. (29) in the form

$$f(\zeta) = 1 + \frac{\mu}{\zeta - d} + \frac{\mu'}{\zeta - d'}\,; \qquad \mu = \frac{(d - c')(d - c)}{d - d'}\,;$$

$$\mu' = \frac{-(d' - c)(d' - c')}{d - d'} \tag{30}$$

and let the new $g(\zeta)$ be written

$$\tilde{g} = 1 + \frac{\tilde{\lambda}_1}{\zeta - d_1} + \frac{\tilde{\lambda}_2}{\zeta - d_2} \cdots \frac{\tilde{\lambda}_N}{\zeta - d_N} + \frac{\tilde{\mu}}{\zeta - d} + \frac{\tilde{\mu}'}{\zeta - d'} + \cdots$$

at least as far as the first-order poles are concerned. Then it is easy to show that

$$\tilde{\lambda}_k = \lambda_k f(d_k); \qquad \tilde{\mu} = \mu g(d); \qquad \tilde{\mu}' = \mu' g(d') \tag{31}$$

with the new closure condition

$$\tilde{\mu} + \tilde{\mu}' + \sum_{k=1}^{N} \tilde{\lambda}_k = 1 \tag{32}$$

Expanding Eq. (32) using Eq. (31) leads immediately to

$$\mu + \mu' + \sum_{k=1}^{N} \lambda_k = 1$$

so that it is necessary to choose

$$\mu + \mu' = 0 \quad \text{or} \quad d + d' = c + c' \qquad (d \neq d') \tag{33}$$

This condition places one constraint only on (c',d') to ensure closure once (c,d) have been selected to achieve the desired effects. Since the higher-order poles do not affect the closure argument, it appears, then, that Eq. (29) [subject to (33)] should be entirely satisfactory.

Some trials were run using the single-pole airfoil (described earlier) as a base configuration with

$$d = 0.7e^{-i30^\circ}$$

This airfoil is fat and highly cambered, but simple. Even so, it was both inconvenient and expensive to make many trials and the three runs described next were the first three using this f-factor. Each configuration was chosen without reference to the results of the preceding choice so that success of these trials is considered adequate demonstration of the flexibility and power of this method.

R1

The first trial (R1) was designed to generate a moderate lump toward the nose of the single-pole airfoil. Thus $|c| > |d|$, $|c| \sim 0.9$ and (c',d') were chosen such that $c' = 0$ while (33) was satisfied. Figure 3a shows the disposition of the poles and zeros, numbers 2 and 3 referring to the additional poles (i.e., d,d'). Figure 3b shows the resulting shape and velocity distribution as a function of normalized surface distance at an orientation corresponding to zero lift. These figures are direct output on the graphics display screen with the exception of formal titles and the crosses denoting the zeros which were added afterwards.

It can be seen that the shape is as expected in both type and location, although the lump is very linear in character having only a very small region of parabolic tip. The velocity shows a very clearly defined blip where expected and, incidentally, the local trailing edge behavior discussed earlier is evident.

R2

This trial was designed to show that putting $|c|$ nearer to the boundary would increase the sharpness and size of the lump. Figures 4a and 4b show that this expectation was

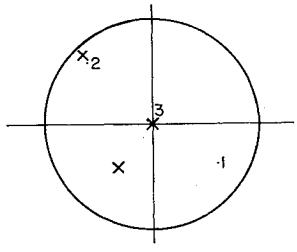

POLE DEFINITIONS CASE RI

NO.	ORD	RADIUS	OMEGA	A	B
1	1	.7	-30.0	.952345	.017734
2	1	.84852	135.0	.004656	-.048617
3	1	.070710	135.0	.042999	.030883

Fig. 3a Case R1: distribution of poles (.) and zeros (x) in the circle plane.

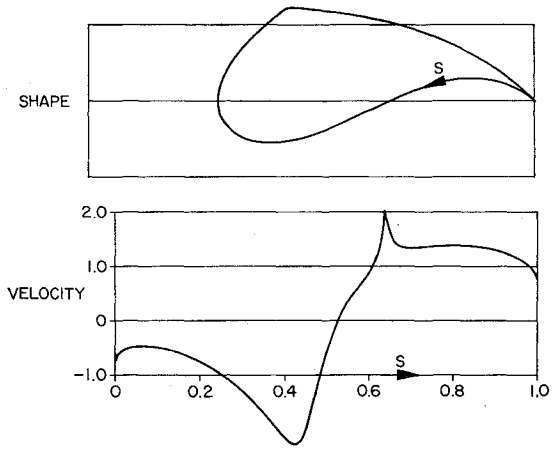

Fig. 3b Case R1: resulting airfoil and velocity distribution at zero lift.

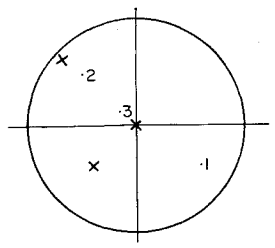

POLE DEFINITIONS CASE R2

NO.	ORD	RADIUS	OMEGA	A	B
1	1	.7	-30.0	.887852	.038593
2	1	.707107	135.0	-.001101	-.186075
3	1	.212132	135.0	.113249	.147482

Fig. 4a Case R2: distribution of poles (.) and zeros (x) in the circle plane.

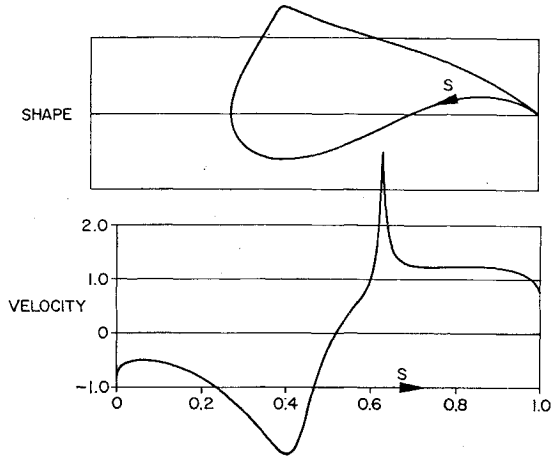

Fig. 4b Case R2: resulting airfoil and velocity distribution at zero lift.

realized. There was a corresponding increase in the velocity blip, although it is only fair to point out that the plotting routine itself joins discrete points with linear segments and only 50 were used on each plot. Hence, the precise "sharpness" of these curves may be deceptive.

R3

According to the arguments put forward earlier, interchanging the radii of c and d should lead to an inward dip. Figure 5a shows the chosen configuration corresponding approximately to a reversal of R1, and Fig. 5b shows that the results are exactly as expected.

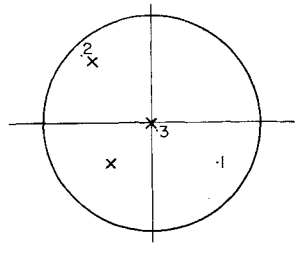

POLE DEFINITIONS CASE R3

NO.	ORD	RADIUS	OMEGA	A	B
1	1	.7	-30.0	1.058905	-.025172
2	1	.919239	135.0	-.005796	.041814
3	1	.070710	-45.0	-.053109	-.016643

Fig. 5a Case R3: distribution of poles (.) and zeros (x) in the circle plane.

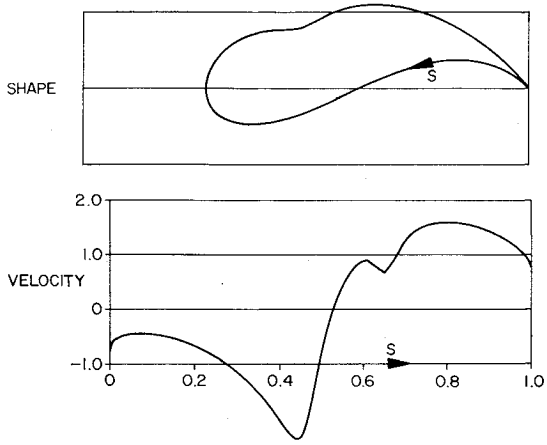

Fig. 5b Case R3: resulting airfoil and velocity distribution at zero lift.

Thus, these results demonstrate that, by using a factor of the form (29), bumps and dips can be generated with associated velocity perturbations more or less at will. An f^2 factor was also tried on the grounds that this should intensify the action of f, and the results obtained corresponding to R1–R3 as above were exactly as expected.[5]

It is clear that this kind of artifice is not possible unless freedom to choose both poles and zeros is available. Hence, the versatility of this system compared with previous generalizations like Von Mises profiles and so on, is not merely an academic detail but a real practical useful feature. Furthermore, the use of the pole airfoil format is not necessarily restricted to generating test problems, but might be of use in the following areas: a) simulation of peculiar airfoils (Griffith, continuously deflected flaps, etc.); b) representation of arbitrary airfoils by a very small number of poles instead of a very large number of surface singularities; c) optimization by manipulation of poles and zeros; d) control of early separation or transition or unduly high velocity peaks by designing dimples.

Conclusions

A consolidation of elementary mapping from circles as a design tool for airfoil test problems has been presented which both simplifies and unifies the theory. Most commonly used test airfoils belong to the wider class (regular) which includes these pole airfoils, and all of the members of the regular airfoil class have trailing edge singularities slightly different from the expected. By exploiting the versatility of the pole airfoil class, it has been shown that local convolutions can be generated to order—a very useful practical facility. In addition, this feature leads to further possibilities enumerated as (a-d) above.

References

[1] Hess, J. L. and Smith, A. M. O., "Calculation of Potential Flow About Arbitrary Bodies," *Progress in Aeronautical Sciences*, Vol. 8, Pergamon Press, New York, 1966.

[2] James, R. M., "A New Look at Two-Dimensional Incompressible Airfoil Theory," MDC-J0918, McDonnell Douglas Corp., Long Beach, Calif.

[3] Catherall, D., Foster, D. N., and Sells, C.C. L., "Two-Dimensional Incompressible Flow Past a Lifting Airfoil," R.A.E. Rept. TR69118, 1969, Royal Aircraft Establishment, Farnborough, Hants, England.

[4] Liebeck, R. H. and Ormsbee, A. I., "Optimization of Airfoils for Maximum Lift," *Journal of Aircraft*, Vol. 7, No. 5, Sept. 1970, pp. 408–415.

[5] James, R. M., "A General Class of Airfoils Conformally Mapped from a Circle," Rept. MDC-J5108, 1971, McDonnell Douglas Corp., Long Beach, Calif.

[6] Carafoli, E., *Zentralblatt für Mechanik*, Vol. 8, 1939, pp. 94.

[7] Piercy, N. A. V., et al., "A New Family of Wing Profiles," *Phil Mag.*, Ser. 7, Vol. XXIV, 1937, pp. 425.

[8] Piercy, N. A. V., et al., "The New Transformed Wing Sections," *Aircraft Engineering*, Nov. 1939, pp. 339.

[9] Rauscher, M., *Introduction to Aeronautical Dynamics*, Wiley, New York, 1953, pp. 304–307.